Green Almond Peels a Promising Biosorbent for Cationic Dyes Removal: Characterization, Effect of Process Parameters and Kinetic Modeling

Souhila Bettayeb[1,2*], Akila Merakchi[1,2], Hakim Lounici[2,3]

[1] Institute of Technology, University of Bouira, 10 000 Bouira, Algeria

[2] Laboratory of Materials and Sustainable Development, Faculty of Science and Applied Sciences, University of Bouira, 10 000 Bouira, Algeria

[3] CRAPC, Research Center in Physico-Chemical Analysis, BP 384 Z.I. Bou-Ismail CP, 42004 Tipaza, Algeria

* Corresponding author's e-mail: s.bettayeb@univ-bouira.dz

ABSTRACT

In the present work, almond peels (AP), an inexpensive and widely available cellulosic material in Algeria, have been utilized as an effective natural adsorbent to eliminate methylene blue from water-based solutions. SEM and FTIR analysis were employed to qualify the adsorbent. The effect of particle size, pH of solution, agitating rate and adsorbent dose were optimized to measure the almond peels capacity of adsorption. The pseudo-first and second-orders, Elovich, and intra-particle diffusion models were employed for analyzing adsorption kinetics. Equilibrium adsorption was examined through Langmuir, Freundlich, and Temkin isotherms. The sorption mechanism was most clearly outlined by the pseudo-second-order kinetic and Freundlich isotherm equations. Our experimental findings indicate that the efficacy of employing these porous adsorbents stems not only from their effective performance attributed to their compositional and structural properties but also from their easy separation from solutions owing to their macroscopic dimensions.

Keywords: almond peels, adsorption, methylene blue, adsorption capacity, isotherms, kinetics.

INTRODUCTION

Dyes find extensive usage for industrial, printing, food, cosmetic and clinical. However, their predominant application in textile industries amounts to their resilience to chemical alterations, simplicity of production, and diversity. Nevertheless, this resistance to degradation leads to environmental contamination when dyes are discharged through effluents.

Globally, over 7.10^5 tons of dyes are generated each year, with nearly 10% being expelled into industrial effluents [Hao et al., 2018; Natarajan et al., 2017] The majority of dyes possess intricate aromatic structures that exhibit stability and resistance to degradation due to light or heat, in spite of presence of oxidizing elements [Li et al., 2014]. Prolonged consumption of water which contain elevated dyes concentrations could

pose mutagenic and carcinogenic risks, and in more critical instances, result in significant harm to the liver, central nervous system and digestive system in humans [El-Zawahry et al., 2016]. Methylene blue (MB) is habitually employed for dyeing cotton, wood and silk. Inspiration of this substance can result respiratory impairment, and direct exposure may lead to lasting damages to the eyes of humans and animals, causing local burns, heightened sweating and mental disorders. Thus, this dye has been used as a model dye for our study. Various technics have been used for the elimination of MB from colored effluents involving adsorption [Tariqul Islam et al., 2018], ion exchange [El-Moselhy et al., 2017], photocatalytic degradation [Ali et al., 2016], flocculation-coagulation [Liang et al., 2014], precipitation [Bayat et al., 2018], biological oxidation [Manenti et al., 2014] and membrane filtration [Li et al., 2017].

The adsorption technique stands out as the most viable option due to its simplified operations, suitability for industrial use, high effectiveness, and abundance of adsorbent materials [Li et al., 2018]. In this sense, numerous investigations have documented the development of economical adsorbents obtained from various agro-industrial rubbish and by-products to remove MB from wastewater including pine cone [Dawood et al., 2017], almond shell [Jabli et al., 2017], banana peels [De Carvalho et al., 2015], peach shell [Markovic et al., 2015], sheep manure waste and sawdust [Dardouri et al., 2017], cashew nut shell [Subramaniam et al., 2015], citrus limetta peel [Shakoor et al.,2016], almond gum [Bouaziz et al., 2015].

In the context of this research, raw almond peel is applied as cheap and powerful adsorbent of MB. The almond trees (prunus dulcis) occupy an area of the order of 132 000 ha in Algeria, for a production of 40 000 Tons of almond in shell per year. So, a considerable amount of green almond peels is generated each year during the collection of prunus dulcis almonds. Apart from its use as a food rich in various nutrients of cattle, almond peels are almost useless. In order to valorize this waste, almond peels were utilized in this study as an efficient, inexpensive, and easy to use adsorbent to eliminate cationic dyes. Moreover, fraction size used in this study [1-3 mm] makes easy the adsorbent separation from aqueous solutions. So, the filtration step isn't required in this case.

MATERIALS AND METHODS

Materials

The dye used was a synthetic Methylene blue provided from BIOCHEM chemopharma laboratory. It has a molecular weight of 319.859 and a formula $C_{16}H_{18}ClN_3S.XH_2O$. With a positive charge, this dye comprises the aromatic section connected to the dimethyl amino group. Figure 1 illustrate the structure of MB [Bagheri et al., 2017];
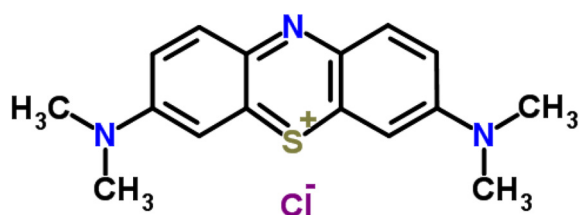
Hydrochloric acid 37% (SIGMA-ALDRICH); Sodium hydroxide (CARLO-ERBA).

Methods

Preparation of the adsorbent

The green almond peels were gathered from Lakhdaria region, Algeria, in August 2017. Then, they were dried in the open area and chopped mechanically in a mixer grinder and sieved. Only fractions of a large diameter were retained (between 0.315 and 6 mm). The fractions were rinsed repeatedly with distilled water till pH 6.5 and no color in the wash water remained. Then, these fractions were subjected to drying in an oven at 40 °C for 48 h and subsequently kept in hermetically sealed glass boxes. The fractions used in the adsorption tests are 0.315–0.5, 0.5–1 mm, 1–3 mm, and 3–6.3 mm.

Preparation of solutions

To prepare the standard MB solution, the right quantity of solid methylene blue is dissolved in distilled water. This solution is utilized to get daughter solutions by dilution. For all adsorption tests, MB solutions concentrating from 10 to 600 mg/l were prepared and used to test adsorption efficiency.

Adsorption test

Tests were accomplished at room temperature (approximately 23 °C) and the procedural steps were as follows: 250 ml of MB solutions differently concentrated is introduced into 400 ml beakers. The correct quantity of adsorbent is subsequently added to these solutions. Then, prepared solutions are stirred at 1000 rpm (magnetic stirring) and samples of 0.5 ml are taken in distinct time intervals (5, 10, 15, 20, 30, 40, 50, 60, 90, 120, 150, 180, 210, 240, 270, and 300 min). The collected solutions are then diluted and examined by UV-visible spectrometry to evaluate the amount of methylene blue remaining at the sampling time, at 664 nm, using a previously determined calibration curve.

The adsorbed quantity of MB is determined by this expression:

$$q_t = \frac{C_0 - C_t}{m} \times v \qquad (1)$$

where: C_0 – the dose of MB at the beginning (mg·l^{-1}), C_t – MB dose at time t, v – the solution volume, m – mass of the adsorbent (g).

Figure 1. The structure of methylene blue

$$q_e = \frac{C_0 - C_e}{m} \times v \qquad (2)$$

where: C_e is the equilibrium concentration of MB.

Adsorbent characterization

Distribution of particle sizes

The economic perspective emphasizes the significance of particle size as a crucial parameter, because of grinding and filtration which involve very high energy consumption. Indeed, the filtration process intended to eliminate the polluted adsorbent requires very fine filters because of the fine size of the particles without forgetting the costs relating to the cleaning of these filters, whereas a simple decantation is sufficient for larger sizes of particles. Therefore, an appropriate size of the adsorbent lowers the operation expenses.

The analysis of AP particle size distribution was conducted employing the AFNOR standard sieve series (French Association of Normalization). First, AP was milled and then separated. AFNOR/size mm: 26/0, 315; 28/0, 5; 31/1; 36/3, 15; 35/ 0.500; 39/6, 3). A simple of 100 g of the milled adsorbent was screened and the fraction at size more than 6.3 mm was eliminated. Then, the mass of AP kept on each sieve was weighed, and percentages of different proportions was calculated.

Zero charge point

To elucidate the role of the charge carried by the adsorbent surface in the fixation of dye, the isoelectric point (pH_{PZC}) of almond peels was determined with the aim of finding the surface charge of this biosorbent. This one corresponds to the value of pH of the medium for which the resulting of the positive and negative charges of surface is null. The pH_{PZC} is a very significant factor in the phenomena of adsorption, particularly when electrostatic forces are implicated in the mechanisms, as is the case with biomasses. Thus, to determine the pH_{PZC}, the tests of pH were realized by a simple and fast method [Ben Ali et al., 2016; Maaloul et al., 2017; Zarghami et al., 2016]. The method consists in putting 50 Cm^3 of a 0.01 M NaCl solution in sealed flasks and modifying the pH of each one (data ranging between 2 and 12) per addition of concentrated NaOH or HCl solutions. In each flask, 0.15 g of adsorbent is introduced. The suspensions are to be consistently agitated, at ambient temperature (23 °C) during 48 h to determine the final pH. The pH_{PZC}

is identified where the curve pH_{final} vs. $pH_{initial}$ intercepts the line $pH_{final} = pH_{initial}$.

AP morphological and structural characterization

To realize the FTIR analysis, a JASCO FT/IR-4200, ATR PRO450-S spectrophotometer was used at maximum resolution of 8 cm^{-1} to make absorbance measurements. The characterization was realized in the interval of 400–4000 cm^{-1} to explore the adsorbent surface features. SEM analysis was employed to depict the fibrillose morphology of the almond peels. Images of the AP surface were obtained using a QUANTA 650 scanning microscope.

RESULTS AND DISCUSSIONS

The adsorbent analysis

Distribution of particle diameter

The particle diameter distribution concerning the particle size of AP material is shown in Table 2. In order to eliminate the filtration step and ease the separation of the adsorbent from aqueous solutions, the fraction used was that of size 1–3 mm. More than 41% of particles have size between 1 and 3 mm, and about 47% of particles have a size less than 1 mm. this distribution can be modified by reducing the grinding time to increase the amount of the fraction used in this study, which means reducing the cost of adsorbent preparation.

Zero charge point

Figure 3 demonstrates that the almond peels pH_{PZC} is equal to 6. The total surface charge is positive when solutions pH is less than 6 but it becomes negative when the pH exceeds the pHPZC. Since the dye employed is basic, its dissolution in water results in the released of cations. Almond peels include polar groups like hydroxyls and carboxyl. Furthermore, the biosorbent electric charge is impacted by the solution hydrogen potential caused by the ionization of these surface functional groups. Mishra et al. (2023) observed that the retention of MB on a biosorbent rises with the augmentation of the negative charge on the surface. This suggests that the retention become more noticeable when the pH surpasses 6. On the other hand, the decrease of efficiency with the augmentation of pH reveals that the reaction is complicated and extends beyond a basic electrostatic attraction occurring between oppositely
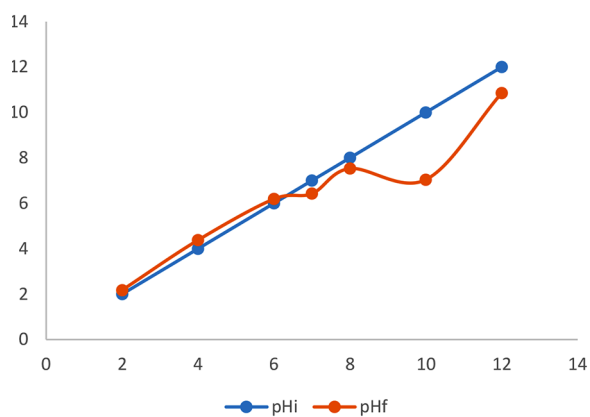
Figure 2. Point of zero charge

Figure 3. FTIR spectra of almond peels after and before adsorption test

charged groups. Indeed, the primary alcohol functionalities present in cellulose and lignin transform into alcoholic functions in the presence of NaOH. This assumption leaves suppose that if the medium becomes highly basic, a rivalry is potential to happen between NaOH and the dye molecules. The Na^+ cations which are very small and more active may prevent the dye ions to reach the adsorbent surface.

AP morphological and structural characterization

The FTIR spectrum of AP, as depicted in Figure 2, reveals several absorption peaks, observed around 3338.17, 2921.63, 1606.41, 1438.63, 1332.57, 1251.57 and 1029.8 cm^{-1}, explaining that various functional groups of the adsorbent could be implicated in the adsorption. The large band about 3338.17 cm^{-1} is imputed to (O-H) and (N-H) group stretching vibration [Tural et al., 2017; Suyog et al., 2018], shifted to 3355.53 cm^{-1} after adsorption. The C–H elongating in aliphatic structures is observed within the interval of 2950–2800 cm^{-1}. Hence, the peak observed in the biosorbent at approximately 2921.63 cm^{-1} may signify the presence of lignin cellulose and hemicellulose rich in aliphatic alkyls and methylene groups CH_2
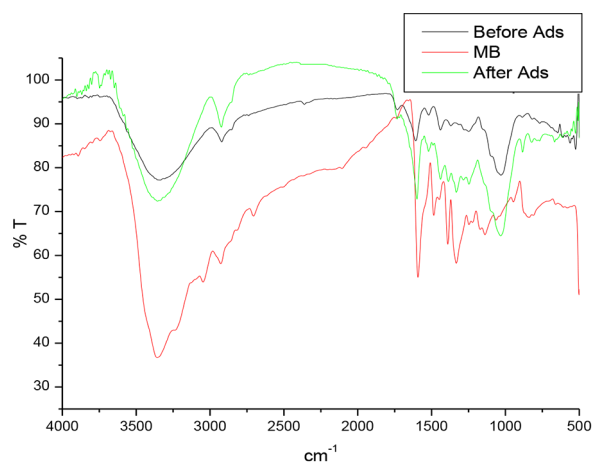
so it must indicate C-H vibration [Kupeta et al., 2018; Yang et al., 2023], shifted to 2923.56 cm^{-1} after adsorption. The band at 1606.41 cm^{-1} suggest the presence of (C=O) stretch vibration and NH_2 stretch bending [Tural et al., 2017; Suyog et al., 2018] shifted to 1598,7 cm^{-1} after adsorption, this band can also be related to aromatic –C=C– and –C=N– stretching [Obakeng et al, 2023, Alver et al., 2020]. The band around 1332 cm^{-1} correspond to –C–N– stretching [Alver et al., 2020]. The peak at 1438.64 cm^{-1} is linked to C-O in carboxylic groups [Erfani et al., 2017]. Certain peaks within the 1370–1310 cm^{-1} range are complex to be assigned but can potentially be linked to C–O stretching in O–C=O constructures, the deformation vibration of surface O-H groups, also to C–N of amides or possibly deformation of C–H bonds [Kupeta et al., 2018; Erfani et al., 2017]. N-H groups can be detected also in this interval [Choudhary et al., 2017]. Peaks at wavenumber 1251 shifted to 1286 cm^{-1} are attributed to the stretching vibration of the C-O band in the ester groups [Debnath et al., 2016]. Finally, the peak at 1030 cm^{-1} may be produced by alcoholic C–O bonds and C-N bonds [Kanakarajua et al, 2018].

Table 1. Functional groups by FTIR analysis

Peak	ν before	ν after	Functional group	Reference
1	3338.18	3355.53	O-H and NH group stretching vibration	[33, 34]
2	2921.63	2923.56	C-H aliphatic and aromatic	[17, 35, 36]
3	1606.41	1598.7	C=O in carboxylic group and NH_2 stretch bending, -C=C- and -C=N-	[32-34, 37, 38]
4	1438.64	1438.63	COO^-, C=O	[39]
5	–	1332.57	COO^-, $C-H_n$, -C-N-	[35, 40]
6	1251.57	1286.29	C-O-R and N–H	[41]
7	1029.8	1031.73	Alcoholic C-O, C-N	[42, 43]

Table 2. Particle size distribution and optimal sorbent dose for the different particle size fractions

Particle size (mm)	% weight	Optimal adsorbent dose (g/l)
<0.315	5.17	–
0.315–0.5	20.13	0.8
0.5–1.0	22.41	2
1.0–3.0	41.92	3
3.0–6.3	10.37	5

This strongly suggests that functional groups including carboxylic and hydroxyl groups play an essential contribution in the sorption of MB on the binding sites.

The SEM pictures show the surface irregularity and a substantial number of cavities/pores where MB dye molecules can accumulate. These images show also that the cavities have different sizes which are considered important for the accessibility of dye molecules. Figure 4 illustrates the scanning electron microscopy images of AP at different magnitudes.

Batch biosorption trials

Stabilization of pH

The stability of pH over time was examined by conducting a test in which a container including 50 ml of bidistilled water with a pH of 6.88 was used. In this beaker, 0.1 g of adsorbent with
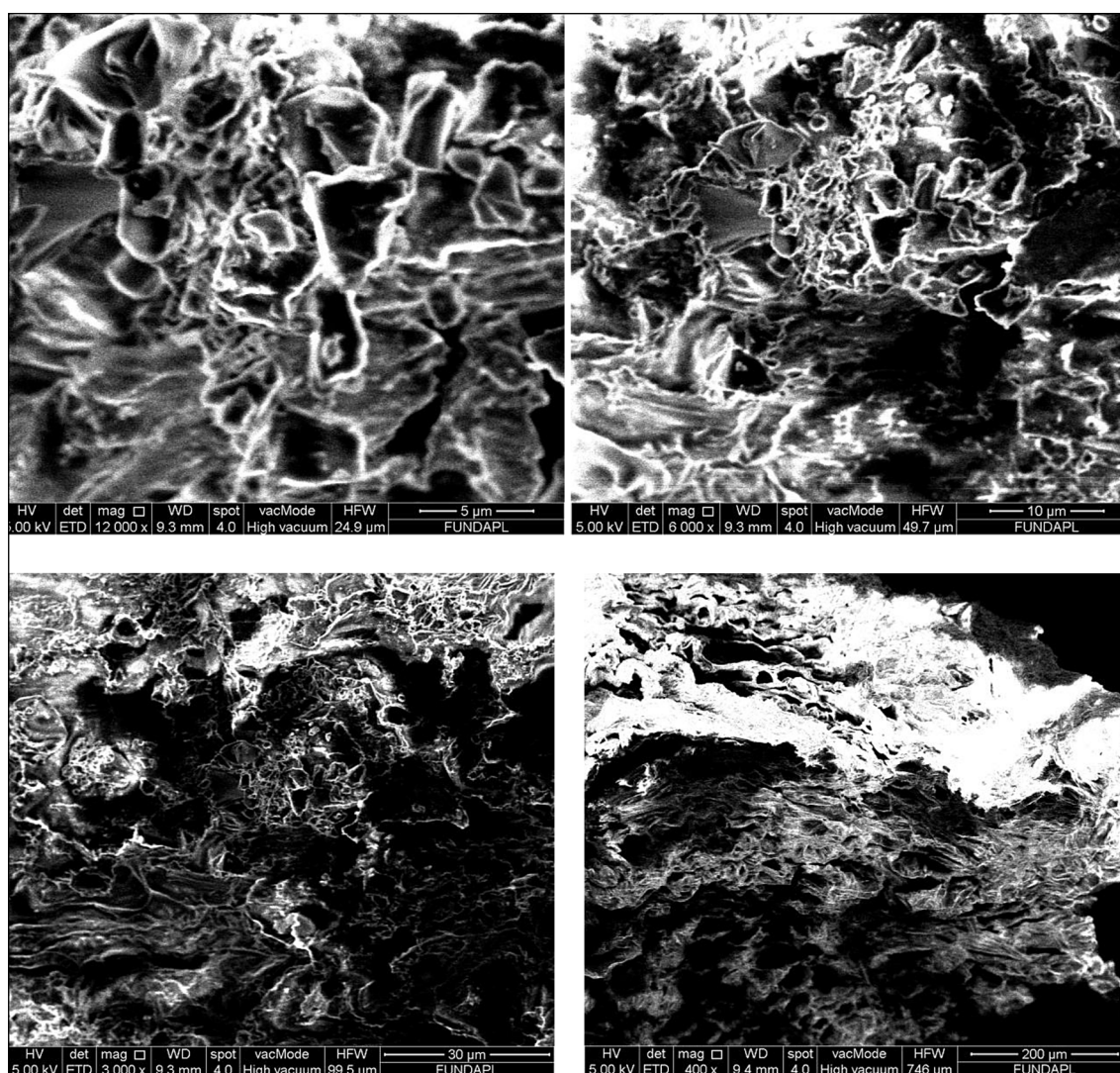
Figure 4. SEM analysis of raw almond peels adsorbent

fraction size 1–3 mm is introduced. The mixture is subjected to magnetic agitation at a rate of 500 rpm and a temperature of 23 °C for a duration of 4 hours. Plotting the pH vs. time curve allows us to predict whether or not the adsorbent releases the protons in solution. For 30 min (Fig. 5), pH decreases from 6.88 to 6, then it increases to 7.2 at 90 min and finally it decreases to 6.78. This implies that during the initial 30 minutes, the adsorbent releases protons. This is followed by the release of hydroxyls in the subsequent hour. After that, it releases protons again until reaching pH of bidistilled water. This change in pH is indicative of ion exchange occurring at the level of the functional groups.

Impact of starting pH (pHi) on MB removal

The solution pH is a fundamental factor which must be studied. In many studies, pH has a decisive role on the adsorption capacity. But in this one, it was proved that this last has no impact on the adsorption capacity of MB. So, we can work at pH of the MB solution (pH = 5.98) and it is a great advantage already that the acidic and basic releases are themselves considered as contaminations. However, at pH = 2.25 (Fig. 6) the equilibrium time is slightly longer (20 min). The adsorption capacity reached is of the order of 3 mg/g for the concentration 10 mg/l.

Impact of agitation

The influence of agitation speed on MB adsorption capacity is also explored. Optimal adsorption capacity is achieved at a stirring speed of 700 rpm (Fig. 7). This moderate speed insured a well-balanced homogeneity for the mixture suspension. Although, beyond this speed the agitation has practically no effect on the adsorption capacity.
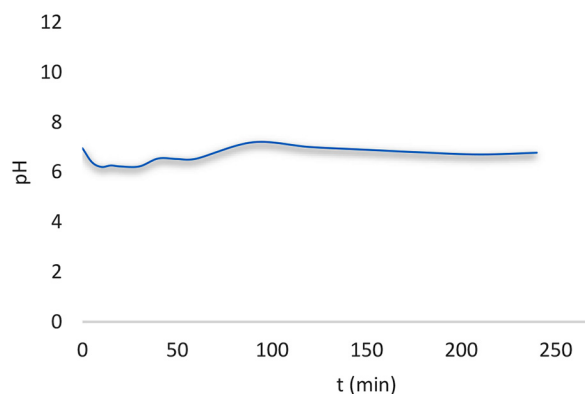
Impact of both particle dimension and MB concentration on the capacity of adsorption

The influence of particle size on the MB adsorbed amount was analyzed. Four size classes were chosen, namely: 0.315–0.5 mm, 0.5–1 mm, 1–3 mm, and 3–6 mm. Figure 8 shows that the redaction of the particle dimension induces a rise in adsorption capacity. In addition, the rise of the starting concentration is concomitant with a boost in the adsorption capacity for each granular fraction. The best capacity obtained is that of the fraction 0.315–0.5 mm (Fig. 8). The value 83.74 mg/g is obtained for the starting concentration 100 mg/l and the residual concentration was 16 mg/l what makes a percentage of elimination about 84%. While, for high concentrations an elevated adsorption capacity is registered (about 142 mg/g) but the residual concentration, which is not represented here, was also important (about 108 mg/l corresponding to an elimination yield about 57% using the fraction 0.315–0.5 mm). In that case, the contamination has not disappeared (43% of pollutant remained). So, the used amount of adsorbent isn't sufficient to eliminate all dye quantity because of the saturation of active sites.

According to these results we can say that almond peels adsorbent is so efficient in MB elimination at medium concentration (100 mg/l) even if the particle size is somewhat high 1–3 mm.

Impact of both particle dimension and the adsorbent mass

Adsorbent dose has a great importance in MB elimination because this determines the optimal amount that gives the best adsorption capacity
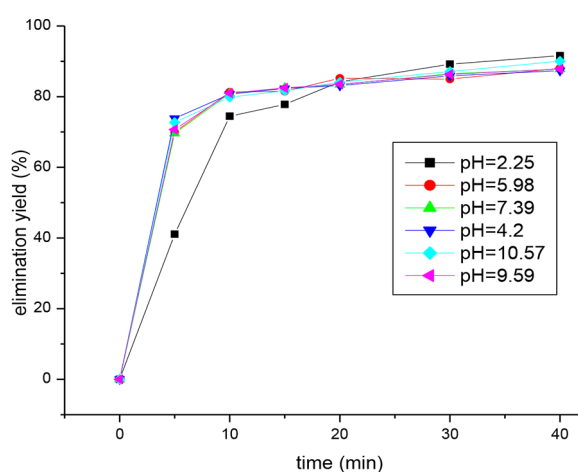

Figure 5. Stabilization of pH

Figure 6. Influence of initial pH on the adsorption capacity: C_0 = 10 mg/l, v = 500 tr/min, pH = 6, m = 5 g/l fraction 1–3 mm

Ecological Engineering & Environmental Technology 2024, 25(2), 351–365

with a minimum of cost. The effect of sorbent dose was investigated for different particle size: 0.315–0.5 mm, 0.5–1 mm, 1–3 mm, 3–6.3 mm with a concentration of 20 mg/l, and pH 6.0. The different quantities of adsorbent used are: 0.1, 0.4, 0.5, 0.6, 0.8, 1, 2, 3, 4, 5, and 6 g/l MB, and the speed of agitation was 700 rpm at 23 °C. The optimal sorbent amount obtained for each fraction is given in table 2 and the effect of both particle size and adsorbent dose is shown in Figure 9.

Impact of both MB concentration and time on adsorption kinetics

The starting dye dose significantly influences its elimination from based-water solutions; it allows the determination of adsorption capacity for a specified initial concentration of MB under operational conditions. The impact of contact time

on the elimination of MB by adsorption was examined at various starting dye dosage using almond peels as adsorbent. Figure 10 shows the obtained results. The findings reveal a proportional increase in the adsorbed amount of MB ranging from 4.1 mg/g to 90.2 mg/g as the initial concentration rises from 10 mg/l to 190 mg/l. Equilibrium is attained within 15 min, 40 min, 150 min and 180 min at concentrations 10, 70, 130, 190 mg/l respectively. Corresponding elimination yield are 82%, 92.4%, 96.8% and 90.2%. At low concentrations, the elimination yield is low because the driving force is feeble compared to the resistance to mass transfer and when the initial concentration augments, this force increase promoting the masse transfer and reducing transfer resistance. Also, it was observed that the time needed to achieve equilibrium increases with the rise in the initial concentration.
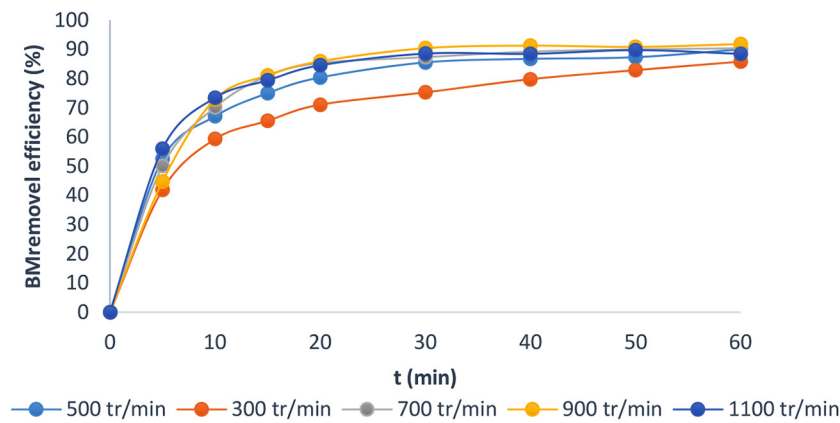
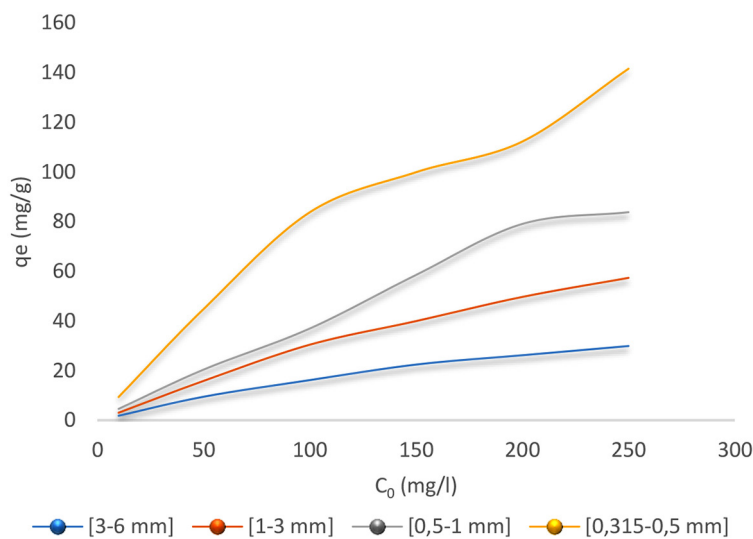**Figure 7.** Effect of stirring on the elimination yield

Figure 8. Influence of particle size and initial concentration on the adsorption capacity of MB (v= 700 rpm, pH = 6)
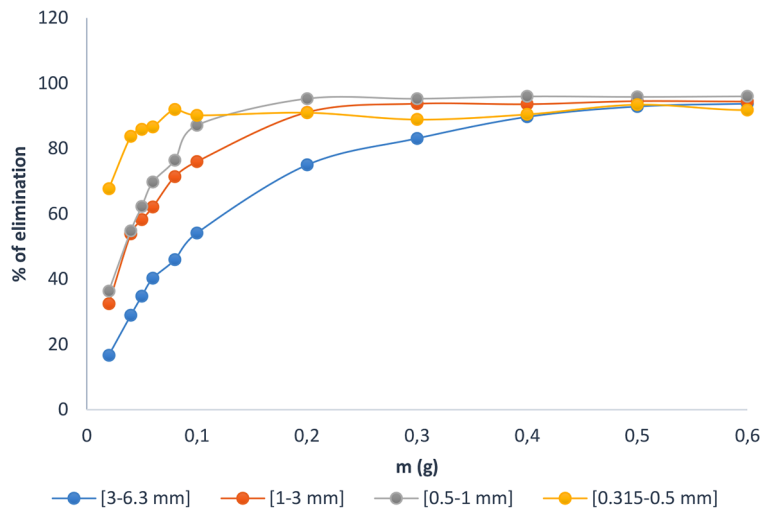
357

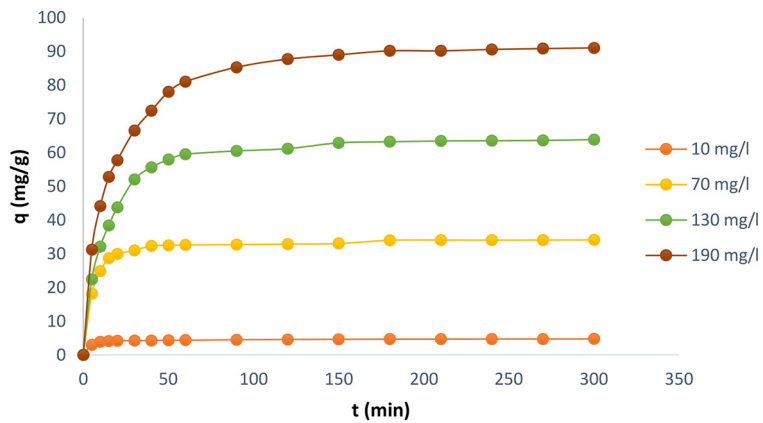**Figure 9**. Influence of adsorbent mass on the dye elimination: v = 700 rpm, pH = 6, C_0 = 20 mg/l

Figure 10. Influence of time and BM concentration on adsorption kinetics:
V = 700 rpm, m = 3 g/l, pH = 6, d = 1–3 mm

Kinetics of MB adsorption

The pseudo first order, pseudo second order and the intra-particle diffusion kinetic models were used to characterize kinetics of MB onto almond peels.

Lagergren pseudo first-order model

The pseudo first order kinetic model is applicable for following adsorption kinetics that occur by diffusion across a frontier. The non-linear from of the pseudo-first-order model is expressed by:

$$q_t = q_e\left(1 - e^{-k_1 t}\right) \qquad (3)$$

where: q_t and q_e – respectively the quantity eliminated at time t and at equilibrium, k_1 – the rate constant of the pseudo first order kinetic model.

A simplified linear pseudo-first-order equation is expressed by the relation (4):

$$log(q_e - q_t) = log(q_e) - \frac{k_1 t}{2.303} \qquad (4)$$

The model constants are found by plotting log $(qe – qt) = f(t)$ given in Figure 11.

Pseudo-second-order model

Instead, the nonlinear form that describe the pseudo second order model for adsorption processes that proceeds by chemisorption is:

$$q_t = \frac{k_2 q_e^2 t}{1 + k_2 q_e t} \qquad (5)$$

where: k_2 (g·mg^{-1}·min^{-1}) – the pseudo second order rate constant.

The linearization of this equation gives:

$$\frac{1}{q_t} = \frac{1}{k_2 q_e^2} + \frac{1}{q_t} t \qquad (6)$$

The values q_e and k_2 are derived based on the slope and intercept of the representation versus t (Fig. 12).
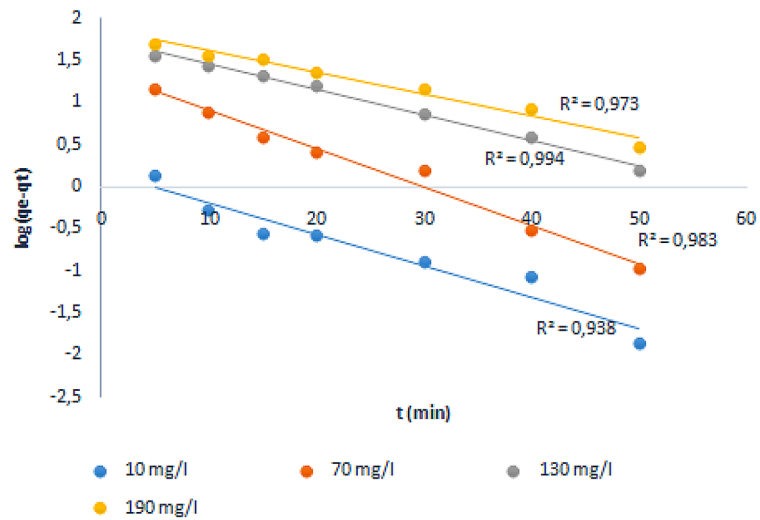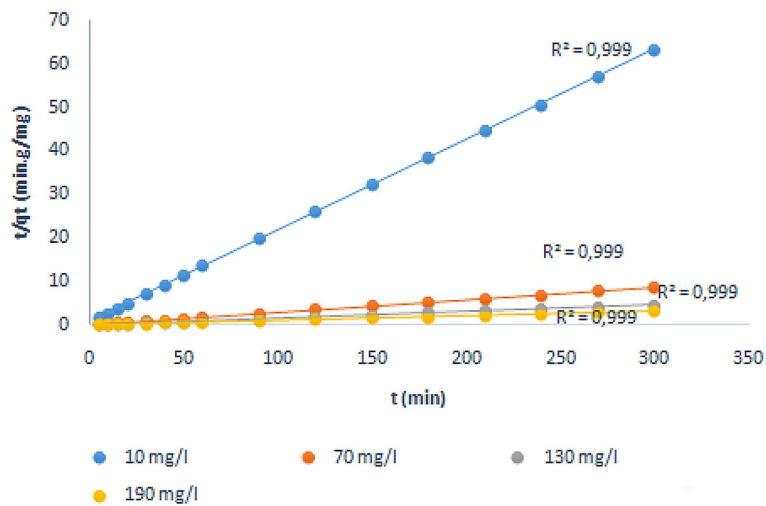
Figure 11. Pseudo-first-order model

Figure 12. Pseudo-second order model

Intra-particle diffusion

The adsorption kinetics were estimated to conceive the mechanisms and rate-controlling steps using the model created by Weber. This model can be aligned with the results found in experiments. The equation of the intraparticle model is:

$$q_t = k_p t^{\frac{1}{2}} + C \qquad (7)$$

where: C – the adsorbed quantity at $t = 0$, k_p – the constant of this model (mg/g min$^{1/2}$).

The slope of the linear representation of this model permits the constant determination. Parameters R^2, k_p and C are given in Table 3.

Based on Figure 13, it seems that the influence of boundary layer diffusion was the origin of adsorption in the initial phases. Subsequently, in the later steps, the intraparticle diffusion impact took place. The intercept from the curve, indicative of the boundary layer impact or influence of the surface adsorption in the rate-controlling stage, exhibited an increase with higher intercept values.

The intraparticle diffusion becomes the exclusive rate-limiting stage when the regression representation of q_t versus $t^{(1/2)}$ is linear and passes through the origine. However, the linear part of the curves at each concentration did not intersect the origin, indicating that intraparticle diffusion alone wasn't the sole step that imposes the most significant restriction on the adsorption rate.

Elovich model

The Elovich model [Pandiarajan et al., 2018] characterizes the chemisorptive attitude between adsorbent and adsorbate. The equation representing this model is:

$$q_t = \frac{1}{\beta}\ln \alpha\beta + \frac{1}{\beta}\ln t \qquad (8)$$

Table 3. Kinetic factors for the removal of MB

Sample	Parameters	10 mg/l	70 mg/l	130 mg/l	190 mg/l
Pseudo first order	k_1 (min^{-1})	0.0852	0.1036	0.0691	0.0576
	qe (mg·g^{-1})	1.202	3.916	5.8	6.46
	R^2	0.938	0.983	0.994	0.973
Pseudo second order	k_2 (g.min^{-1}·mg^{-1})	$5.12 \cdot 10^{-2}$	$7.65 \cdot 10^{-3}$	$1.717 \cdot 10^{-3}$	$8.197 \cdot 10^{-4}$
	qe (mg·g^{-1})	4.78	34.48	66.67	100
	R^2	0.999	0.999	0.999	0.999
Elovich's parameters	α (g^{-1}·min^{-1}·mg)	308.35	144.23	17.18	7603.13
	β (mg^{-1}·g)	2.42	0.234	0.0757	0.123
	R^2	0.841	0.814	0.95	0.934
Intra-particle diffusion model	k_i (g^{-1}·min$^{-0,5}$·mg)	0.074	0.63	2.133	3.42
	C (mg·g^{-1})	3.649	25.27	33.99	42.53
	R^2	0.695	0.552	0.689	0.777

where: α (mg g^{-1} min^{-1}) – the initial adsorption rate, β (mg g^{-1}) – the degree of the surface coverage and activation energy involved in the chemisorptive mode of interaction between the adsorbate and adsorbent.

If the attraction forces between the adsorbate and adsorbent conforms to the Elovich model, the chemisorptions kinetics will exhibit linearity. By constructing a linear representation of qt versus ln(t), the values for $1/\beta$ and $(1/\beta)\cdot\ln(\alpha\beta)$ can be derived. The parameter $1/\beta$ signifies the number of available sites for adsorption, while the $(1/\beta)\cdot\ln(\alpha\beta)$ value denotes the adsorbed mass when ln(t) equals zero. The regression coefficients (R^2) of the Elovich model were relatively low (Fig. 14) suggesting a limited fit to the experimental kinetic results. The different parameters of each model are given in Table 3.

Adsorption isotherms

The adsorption isotherm plays a crucial role in comprehending the mechanism of adsorption.

It explains how molecules of adsorbate are shared between the liquid and the solid phase. Various adsorption isotherms are employed to establish a correlation of the adsorption equilibrium in dye adsorption on diverse adsorbents. Among the famous isotherms are: the Langmuir and Freundlich models [Sadeek et al., 2015].

Figure 15 illustrates the change of adsorption capacity versus equilibrium concentration at tow temperatures: 20 °C and 40 °C. The isotherm observed appears to be of type I. Type I isotherms are associated with microporous solids possessing comparatively minor external surfaces, where the maximum uptake being controlled by the reachable micropore volume instead of the internal surface area. The traditional interpretation of this isotherm suggests adsorption for a complete molecular monolayer. Equilibrium results obtained for the adsorption of MB on almond peels biosorbent have also been subjected to analysis using different isotherms including Freundlich, Langmuir and Temkin.
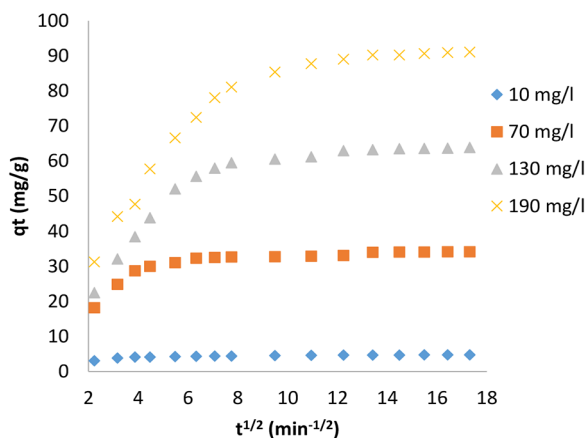

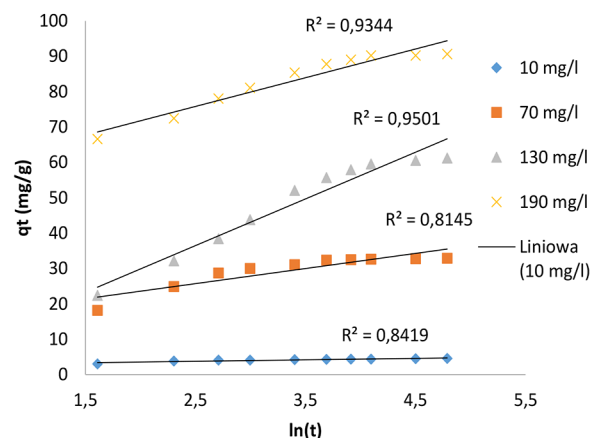**Figure 13**. Intra-particule diffusion model

Figure 14. Elovich model

Freundlich isotherm

The Freundlich model is describes adsorption on non-homogeneous surfaces, taking into account the connection between adsorbed molecules. This empirical equation is used for understanding heterogeneous systems and is expressed as:

$$q_e = K_F C_e^{\frac{1}{n}} \qquad (9)$$

The Freundlich isotherm linear form is presented by the formula:

$$\ln qe = \ln k_f + \frac{1}{nf}\ln C_e \qquad (10)$$

where: q_e – the amount adsorbed at equilibrium (mg/g), K_F – is Freundlich constant [(mg/g)(L/mg)1/n].

This constant describes the related adsorption ability of the biosorbent in relation with the cohesive energy. It is moreover referred to as the distri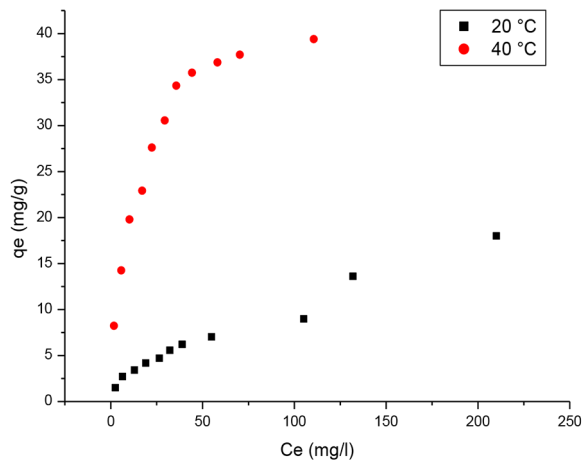bution coefficient, representing the volume of MB ions sorbed onto the adsorbent per unit concentration at equilibrium. While, n expresses the heterogeneity parameter that elucidates the variability in the linearity of adsorption. The adsorption is linear, if $n = 1$; it is physical, if $n > 1$; and it becomes chemical if $n < 1$.

The graphical representation (Fig. 16) of $\ln(q_e)$ versus $\ln(C_e)$ is a linear pattern with a certain incline 1/n and $\ln(K_F)$ at intercept of the linear plot of $\ln(q_e)$ versus $\ln(C_e)$.

Langmuir isotherm

Langmuir isotherm is based on two key assumptions about the adsorption process. First, it posits that adsorption takes place at defined, homogeneous adsorption sites within the adsorbent. Second, it suggests that monolayer adsorption and maximum adsorption happen when adsorbed molecules create a fully filled layer on the surface of adsorbent. In this model, all adsorption sites are supposed to possess the same energy and the intermolecular strength diminishes as the distance from the adsorption surface rises [Ribeiro et al., 2023]. Langmuir model is given as follows:

$$q_e = \frac{q_{max}KC_e}{1+K_L C_e} \qquad (11)$$

The linearization of Langmuir isotherm gives the equation:

$$\frac{C_e}{q_e} = \frac{1}{q_{max}k_L} + \frac{C_e}{q_{max}} \qquad (12)$$

where: C_e (mg/l) – the equilibrium concentration, q_e (mg/g) – is the MB adsorbed quantity at equilibrium, qmax is the maximal MB adsorbed quantity, K_L – is the Langmuir constant (l/mg).

Figure 15. Adsorption isotherms at 40 and 20 °C
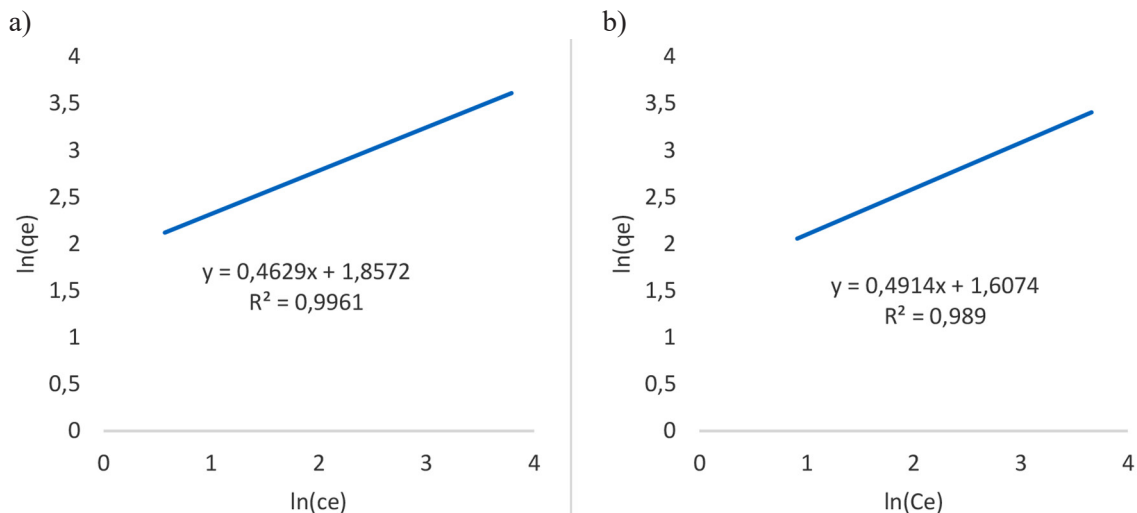
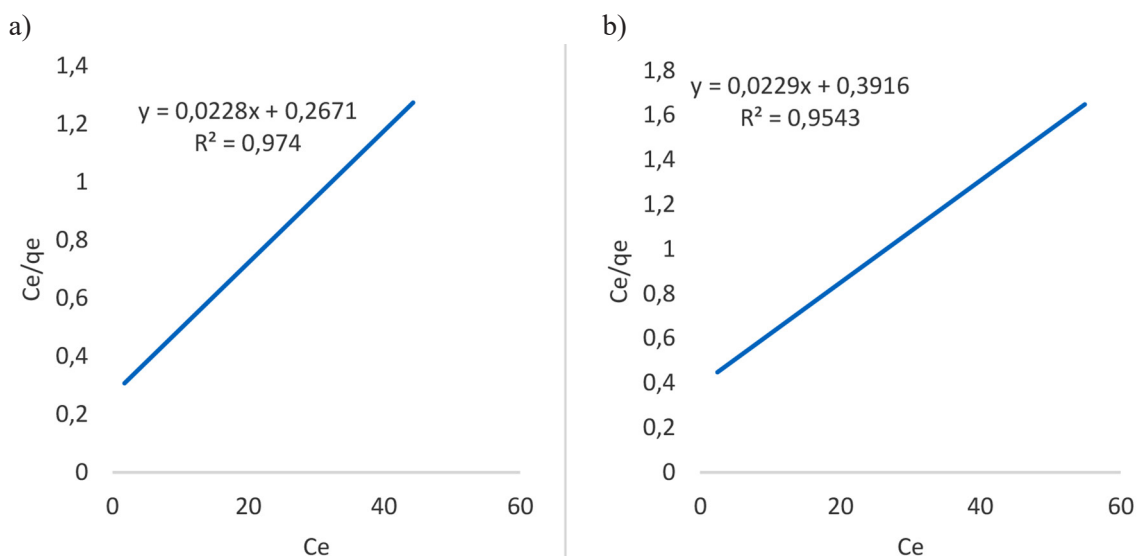**Figure 16**. Freundlich isotherm at (a) 40 °C, (b) 20 °C

a)

b)

Figure 17. Langmuir isotherm at (a) 40 °C and (b) 20 °C

The Langmuir isotherm plot is given in Figure 17.

Temkin isotherm

According to the Temkin isotherm expression, the adsorption energy of the entirety of molecules diminishes in a straight line with the distance between the adsorbent surface and the layer on which the molecule is adsorbed, owing to adsorbent–adsorbate interactions. In addition, the adsorption is distinguished by a homogenous dispensation of the attraction forces, reaching some maximum intensities. Plotting q_e versus $\ln(C_e)$ (Fig. 18) allows for the finding of the isotherm constants B_T and K_T from the slope and the intercept. In the order given, K_T represents the equilibrium binding constant (l·mol⁻¹) related to the peak energy levels, while constant B_T is associated to the heat of adsorption. Temkin model is expressed by:

$$q_e = B_T \ln(K_T C_e) \qquad (13)$$

The determined values of R^2, isotherm constants for each model and relative error data are illustrated in Table 4. R^2 calculated ones for Freundlich isotherm (0.996) were found nearer to unity compared to R^2 values of Langmuir (0.974) and Temkin isotherm (0.959). The examination of trial and modeled data of the equilibrium adsorption capacities at varied circumstances from isotherm models has been represented in Figure 19. It is as well evident from Figure 19 that modeled data of equilibrium adsorption capacity employing the Freundlich isotherm are approximate to the values observed in experiments. The relative error values for the Freundlich isotherm were notably lower compared to those of Langmuir and Temkin isotherms, as indicated from Table 4. The found results affirm that the Freundlich model provides an improved match to the equilibrium data compared to the Langmuir and Temkin isotherms. The Freundlich model is suitable for a solid having surfaces with energetic heterogeneity at

Table 4. Isotherms parameters

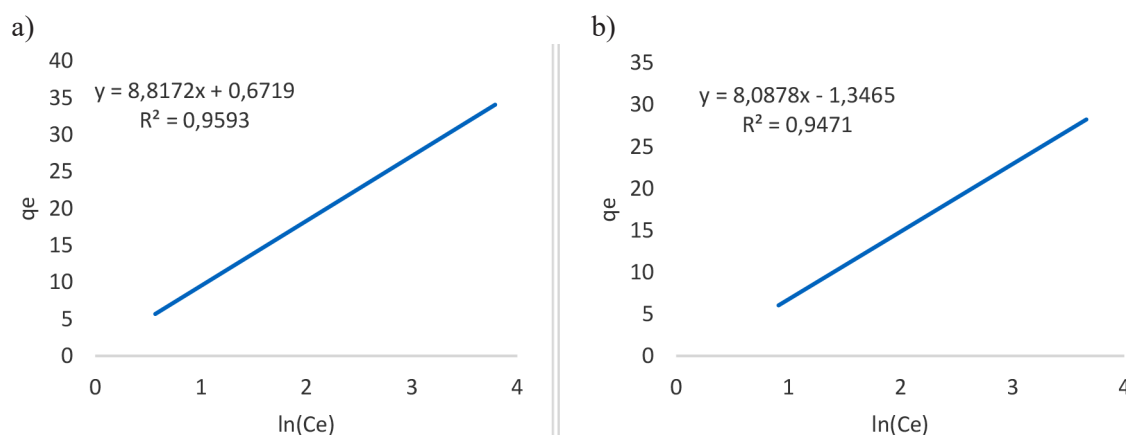| Model	Parameters	20°C	40°C
Experimental	Q_m (mg/g)	31.1	34.34
Freundlich	n	2.04	2.16
	K_F ((mg/g)(l/mg)$^{1/n}$)	4.99	6.52
	R^2	0.989	0.996
Langmuir	Q_m (mg/g)	45.45	45.45
	K_L (l/mg)	0.056	0.082
	R^2	0.954	0.974
Temkin	B	8.087	8.818
	K_T (l/mg)	0.85	1.08
	R^2	0.947	0.959

a)

b)

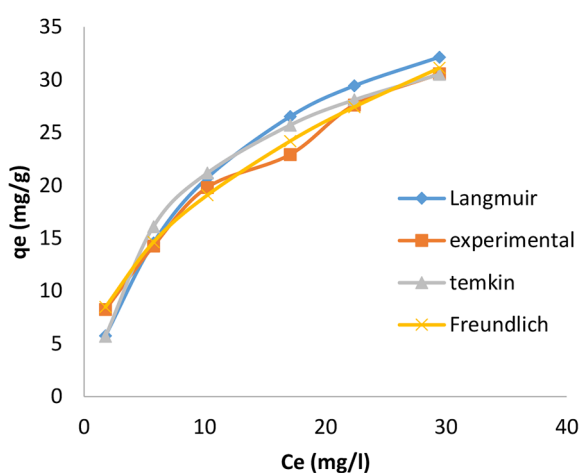**Figure 18**. Temkin isotherm at (a) 40 °C and (b) 20 °C

Figure 19. Comparison between calculated and experimental adsorption capacities

monolayer filling and this holds true in the present study. It is noteworthy that, as noticed from Table 4, *Kf* values increased from 4.99 at 293 K to 6.52 l/mg at 313 K, indicating the heat-absorbing nature of the adsorption operation.

CONCLUSIONS

The findings indicate that AP can serve as an efficient sorbent for the elimination of MB from based water solutions. In the batch investigation of adsorption variables, except the pH of solution which had no effect on adsorption tests, all of the other factors like: particle dimension, adsorbent dose, time of adsorption and initial MB concentration were identified as crucial factors influencing the biosorption process. Kinetic analysis demonstrated that equilibrium in the adsorption of MB on AP was attained in 10 min for low concentrations and 60 to 90 min for high concentrations. The adsorption process by AP adsorbent was well-represented by the Freundlich isotherm, and the pseudo-second-order kinetics demonstrated to be a suitable model for the rate of sorption.

REFERENCES

1. Ali L. I., El-Molla S. A., Ibrahim M. M., Mahmoud H. R., Naghmash M. A. 2016. Effect of preparation methods and optical band gap of ZnO nanomaterials on photodegradation studies Optical Materials (58) 484-490

2. Alver E., Metin A.Ü., Brouers F. 2020. Methylene blue adsorption on magnetic alginate/rice husk bio-composite, *International Journal of Biological Macromolecules*, https://doi.org/10.1016/j.ijbiomac.2020.02.330

3. Bagheri A.R., Ghaedi M., Asfaram A., Jannesar R., Goudarzi A., 2017. Design and construction of nanoscale material for ultrasonic assisted adsorption of dyes: application of derivative spectrophotometry and experimental design methodology, Ultrasonics sonochemistry (35) 112-123.

4. Bayat M., Javanbakht V., Esmaili J. 2017. Synthesis of zeolite/nickel ferrite/sodium alginate bionanocomposite via a co-precipitation technique for efficient removal of water-soluble methylene blue dye. The address for the corresponding author was captured as affiliation for all authors. Please check if appropriate. Biomac, doi:10.1016/j.ijbiomac.2018.05.012

5. Ben Ali S., Jaouali I., Souissi-Najar S., Ouederni A. 2016. Characterization and adsorption capacity of raw pomegranate peel biosorbent for copper removal, Journal of Cleaner Production, https://doi.org/10.1016/j.jclepro.2016.10.081.

6. Bouaziz F., Koubaa M., Kallel F., Chaari F., Driss D., Ellouz Ghorbel R., Ellouz Chaabouni S. 2015. Efficiency of almond gum as a low-cost adsorbent for methylene blue dye removal from aqueous solutions. Industrial Crops and Products (74) 903–911

7. Choudhary B.C., Paul D., Borse A.U., Garole D.J. 2017. Surface functionalized biomass for adsorption and recovery of gold from electronic scrap and refinery wastewater, *Separation and Purification Technology*, https://doi.org/10.1016/j.seppur.2017.12.024

8. Dardouri S., Sghaier J. 2017. A comparative study of adsorption and regeneration with different agricultural wastes as adsorbents for the removal of methylene blue from aqueous solution, doi:10.1016/j.cjche.2017.01.012

9. Dawood S., Kanti T., Phan S.C. 2017. Synthesis and characterization of slow pyrolysis pine cone bio-char in the removal of organic and inorganic pollutants from aqueous solution by adsorption: Kinetic, equilibrium, mechanism and thermodynamic. Bioresource Technology. https://doi.org/10.1016/j.biortech.2017.07.019

10. De Carvalho H. P., Huang J., Zhao M., Liu G., Dong L., Liu X. 2015. Improvement of Methylene Blue removal by electrocoagulation/ banana peel adsorption coupling in a batch system, Alexandria Eng. J. http://dx.doi.org/10.1016/j.aej.2015.04.003

11. Debnath S., Ballav N, Maity A., Pillay K. 2016. Competitive adsorption of ternary dye mixture using pine cone powder modified with β-cyclodextrin, *Journal of Molecular Liquids*, doi: 10.1016/j.molliq.2016.10.109

12. El-Moselhy M. M., M. Kamal S. 2017. Selective Removal and preconcentration of methylene blue from polluted water using cation exchange polymeric material, Groundwater for Sustainable Development, https://doi.org/10.1016/j.gsd.2017.10 .001

13. El-Zawahry M.M., Abdelghaffar F., Abdelghaffar R.A., Hassabo A.G. 2016. Equilibrium and kinetic models on the adsorption of Reactive Black 5 from aqueous solution using Eichhornia crassipes/chitosan composite, Carbohydr. Polym. (136) 507–515.

14. Hao. H, Wang. Y, Shi. B, Han. K, Zhuang. Y, Kong. Y, Huang. X 2018. Strong enhancement of methylene blue removal from binary wastewater by in-situ ferrite process. Journal of environmental science, https://doi.org/10.1016/j.jes.2018.01.019

15. Jabli M., Gamha E., Sebeia N., Hamdaoui M. 2017. Almond shell waste (Prunus dulcis): Functionalization with [dimethy-diallylammonium-chloride-di-allylamin-co polymer] and chitosan polymer and its investigation in dye adsorption, *Journal of Molecular Liquids.* doi:10.1016/j.molliq.2017.05.041

16. Jain S. N., Gogate P. R. 2018. Efficient removal of Acid Green 25 dye from wastewater using activated Prunus Dulcis as biosorbent: Batch and column studies Journal of Environmental Management (210) 226-238

17. Kanakarajua D., Rusydah N., Shahdada M., Limb Y., Pace A. 2018. Magnetic hybrid TiO2/Alg/FeNPs triads for the efficient removal of methylene blue from water Sustainable Chemistry and Pharmacy (8) 50–62

18. Kupeta A.J.K., Naidoo EB., Ofomaja AE. 2018. kinetics and equilibrium study of 2-nitrophénol adsorption onto polyurethane cross-linked pine cone biomass, Journal of cleaner product doi:10.1016/j.jclepro.2018.01.034

19. Li Q., Li Y., Ma X., Du Q., Sui K., Wang D., Wang C., Li H., Xia Y. 2017. Filtration and adsorption properties of porous calcium alginate membrane for methylene blue removal from water Chemical Engineering Journal (316) 623–630

20. Li Y., Sun J., Du Q., Zhang L., Yang X., Wu S., Xia Y., Wang Z., Xia L., Cao A. 2014. Mechanical and dye adsorption properties of graphene oxide/chitosan composite fibers prepared by wet spinning, Carbohydr. Polym. (102) 755–761

21. Li Y., Zhang Y., Zhang Y., Wang G., Li S., Han R, Wei W. 2018. Reed biochar supported hydroxyapatite nanocomposite: Characterization and reactivity for methylene blue removal from aqueous media. Journal of Molecular Liquids, (263) 53-63

22. Liang C. Z., Sun S.P., Li F. Y., Ong Y.K., Chung T.S. 2014. Treatment of highly concentrated wastewater containing multiple synthetic dyes by a combined process of coagulation/flocculation and nanofiltration, J. Membr. Sci. (469) 306–315.

23. M Erfani, V Javanbakht. 2017. Methylene Blue removal from aqueous solution by a biocomposite synthesized from sodium alginate and wastes of oil extraction from almond peanut. The address for the corresponding author was captured as affiliation for all authors. Please check if appropriate. Biomac, doi:10.1016/j.ijbiomac.2018.03.003

24. Maaloul N., Oulego P., Rendueles M., Ghorbal A., Diaz M. 2017. Novel biosorbents from almond shells: Characterization and adsorption properties modeling for Cu(II) ions from aqueous solutions, Journal of Environmental Chemical Engineering http://dx.doi.org/10.1016/j.jece. 2017.05. 037

25. Manenti D.R., Modenes A.N., Soares P.A., Espinoza-Quinones F.R., Boaventura R.A.R., Bergamasco R., Vilar V.J.P. 2014. Assessment of a multistage system based on electrocoagulation, solar photo-Fenton and biological oxidation processes for real textile wastewater treatment, Chem. Eng. J. (252) 120–130.

26. Mishra A, Ojha H., Pandey J., Tiwari A. K., Pathak M. 2023. Adsorption characteristics of magnetized biochar derived from *Citrus limetta* peels. Heliyon 9 e20665

27. Natarajan. S, Bajaj. H.C., Tayade, R.J., 2017. Recent advances based on the synergetic effect of adsorption for removal of dyes from waste water using photocatalytic process. J. Environ. Sci. https://doi.org/10.1016/j.jes.2017.03.011

28. Obakeng B., Saheed N., Sanni O., Viljoen E. L., Pholosi A., Pakade V. E. 2023. Surfactant-modified *Macadamia* nutshell for enhancement of methylene blue dye adsorption from aqueous media, Case Studies in Chemical and Environmental Engineering 8 100357

29. Pandiarajan A., Kamaraj R., Vasudevan S., Vasudevan S. OPAC. 2018. (Orange Peel Activated Carbon) derived from waste orange peel for the adsorption of Chlorophenoxyacetic Acid herbicides from water: Adsorption isotherm, kinetic modelling and thermodynamic studies, Bioresource Technology. doi: https://doi.org/10.1016/j.biortech.2018.04.005

30. Ribeiro. J.P, Cruz. N. C, Neves M. C, Rodrigues. S. M, L. A.C. Tarelho L. A.C, Nunes. M. I 2023. Granulated biomass fly ash coupled with fenton process for pulp and paper wastewater treatment Environmental Pollution 317 120777

31. S Markovic, A Stankovic, Z Lopici, S Lazarevic, M Stojanovic, D Uskokovic. Application of raw peach shell particles for removal of methylene blue. J. Environ. Chem. Eng. (2015), http://dx.doi.org/10.1016/j.jece.2015.04.002

32. Sadeek S. A., Negm N. A., Hefni H.H.H., Abdel Wahab M. M. 2015. Metal adsorption by agricultural biosorbents: Adsorption isotherm, kinetic and biosorbents chemical structures. International Journal of Biological Macromolecules (81) 400–409

33. Shakoor S., Nasar A. 2016. Removal of methylene blue dye from artificially contaminated water using citrus limetta peel waste as a very low-cost adsorbent Journal of the Taiwan Institute of Chemical Engineers (000) 1–10

34. Subramaniam R., Ponnusamy S. K. 2015. Novel adsorbent from agricultural waste (cashew NUT shell) for methylene blue dye removal: Optimization by response surface methodology Water Resources and Industry (11) 64–70

35. Tariqul Islam M., Saenz-Arana R., Hernandez C., Guinto T., Ariful Ahsan M., Bragg D. T., Wang H., Alvarado-Tenorio B., Noveron J. C. 2018. Conversion of waste tire rubber into a high-capacity adsorbent for the removal of methylene blue, methyl orange, and tetracycline from water, Journal of Environmental Chemical Engineering https://doi.org/10.1016/j.jece.2018.04. 058

36. Tural B., Ertas E., Enez B., Ag*u*loglu Fincan S., Tural S. 2017. Preparation and characterization of a novel magnetic biosorbent functionalized with biomass of Bacillus Subtilis: Kinetic and isotherm studies of biosorption processes in the removal of Methylene Blue, Journal of Environmental Chemical Engineering http://dx.doi.org/10.1016/j.jece.2017.09 .019

37. Yang P., Lu Y., Zhang H., Li R., Hu X., Shahab A., Elnaggar A. Y., Alrefaei A. F., Almutairi M. H., Ali E. 2023. Effective removal of methylene blue and crystal violet by low-cost biomass derived from eucalyptus: Characterization, experiments, and mechanism investigation, *Environmental Technology & Innovation,* doi:https://doi.org/10.1016/j.eti.2023.103459

38. Zarghami, Z., Akbari, A., Latifi, A.M., Amani, M.A. 2016. Design of a new integrated Chitosan PAMAM Dendrimer biosorbent for heavy metals removing and study of its adsorption kinetics and thermodynamics, *Bioresource Technology*, doi:http://dx.doi.org/10.1016/j.biortech. 2016.01.052